Photochemistry of Framework-Supported M(diimine)(CO)$_3$X Complexes in 3D Lithium-Carboxylate Metal−Organic Frameworks: Monitoring the Effect of Framework Cations.

Thomas J. Reade[1], Thomas S. Murphy[1], James A. Calladine[1], Raphael Horvath[1], Ian P. Clark[2], Gregory M. Greetham[2], Michael Towrie[2],William Lewis[1], Michael W. George[1,3*] and Neil R. Champness[1]*

[a] University of Nottingham, School of Chemistry, Nottingham, NG7 2RD, England.

[b] STFC Rutherford Appleton Lab, Central Laser Facility, Didcot, OX11 0QX, Oxon, England.

[c] University of Nottingham Ningbo China, Department of Chemistry & Environmental Engineering, Ningbo 315100, Zhejiang, Peoples Republic of China.

Abstract

The structures and photochemical behaviour of two new metal-organic frameworks are reported. Reaction of Re(2,2′-bipy′-5,5′-dicarboxylic acid)(CO)$_3$Cl or Mn(2,2′-bipy′-5,5′-dicarboxylic acid)(CO)$_3$Br with either LiCl or LiBr, respectively, produces single crystals of {Li$_2$(DMF)$_2$[(2,2′-bipy′-5,5′-dicarboxylate)Re(CO)$_3$Cl]}$_n$ (**ReLi**) or {Li$_2$(DMF)$_2$[(2,2′-bipy′-5,5′-dicarboxylate)Mn(CO)$_3$Br]}$_n$ (**MnLi**). The structures formed by the two MOFs comprise one-dimensional chains of carboxylate-bridged Li(I) cations that are cross-linked by units of Re(2,2′-bipy′-5,5′-dicarboxylate)(CO)$_3$Cl (**ReLi**) or Mn(2,2′-bipy′-5,5′-dicarboxylate)(CO)$_3$Br (**MnLi**). The photophysical and photochemical behaviour of both **ReLi** and **MnLi** are probed. The rhenium-containing MOF, **ReLi**, exhibits luminescence and the excited state behaviour, as established by time-resolved infra-red measurements, are closer in behaviour to that of unsubstituted [Re(bipy)(CO)$_3$Cl] rather than a related MOF where the Li(I) cations are replaced by Mn(II) cations. These observations are further supported by DFT calculations. Upon excitation **MnLi** forms a dicarbonyl species which rapidly recombines with the dissociated CO, in a fashion consistent with the majority of the photoejected CO not escaping the MOF channels.

Introduction

The field of metal-organic frameworks, or MOFs, has developed rapidly over the past twenty years, building from the original concepts of the building-block approach the field has developed to a position where there are a large variety of framework structures which are being applied to a myriad of applications.[1] Although there are still significant synthetic challenges in the delivery of target MOF structures it is often possible to design and then prepare MOFs that incorporate specific chemical species such that particular properties can be developed. Thus, in addition to studies that exploit the porosity of MOFs for gas storage[2,3] developments have been made in a number of other areas including biological applications,[4-6] conductivity[7] and redox processes,[8] crystalline sponges[9] and as matrices for probing chemical reactions.[10]

One area that has emerged over recent years is the incorporation of photoactive components within MOFs[11,12] whose properties can be subsequently exploited. A variety of different photoactive components have been targeted including systems with photoactive ligands,[13] but also systems where photoactive moieties such as $[Ru(bipy)_3]^{2+}$ [14] and more importantly for this particular study, $M(CO)_3X(diimine)$ (M = Re, Mn) groups have been studied.[15-19] Indeed, both $Re(CO)_3X(diimine)$[15] and $Mn(CO)_3X(diimine)$[16] have been employed for the photocatalytic reduction of CO_2.

Our studies have developed the concept of introducing $M(CO)_3X(diimine)$ (M = Re, Mn) species into MOFs and then studying the photophysical properties of this moiety. Our strategy has exploited a divergent multifunctional dicarboxylate ligand which is also capable of binding a supported metal complex, in our studies 2,2′-bipyridine-5,5′-dicarboxylate (**1**). This approach has been successfully demonstrated by employing $M(\mathbf{1})(CO)_3X$ (M = Re, Mn, X = Cl, Br) as a ligand in the construction of MOFs, with the carboxylate donors of the 2,2′-bipyridine-5,5′-dicarboxylate ligand binding either Mn(II)[17,18] or Cu(II)[19]. Thus the $M(diimine)(CO)_3X$ unit is supported by the extended framework whilst not being involved in the propagation of the MOF structure.

Studies of the MOF-supported $Re(diimine)(CO)_3Cl$ moiety in $\{Mn(DMF)_2[(\mathbf{1})Re(CO)_3X]\}_n$ **ReMn** (Figure 1a) reveal the initial formation of both ^{3}MLCT and ^{3}IL (intraligand) π-π^* states, however, the MLCT bands decay rapidly (*ca.* 20 ps) concurrent with further growth of the intraligand $^3\pi$-π^*. Further, the Time-Resolved Infra-Red (TRIR) spectra obtained 1 ns after laser excitation shows only the presence of intraligand $^3\pi$-π^* states. Interestingly the $^3\pi$-π^* state of $Re(bpy)(CO)_3Cl$ is not normally accessible in

solution as it is higher in energy than the commonly observed ^{3}MLCT state and therefore there is a clear influence of the MOF environment on the nature of the excited states of the framework-supported complex. Further investigation of the tethered M(diimine)(CO)$_3$X complexes indicate that under suitable conditions it is possible to induce isomerisation of the M(diimine)(CO)$_3$X. Thus, prolonged irradiation of {Mn(DMF)$_2$[(**1**)Re(CO)$_3$X]}$_n$ **ReMn**, at 200 K, leads to the observation of free CO hosted in the MOF. Subsequent warming to above 250K leads to the formation of the corresponding *mer*-isomer of the M(diimine)(CO)$_3$X species. In the case of the Re(diimine)(CO)$_3$X containing MOF *ca*. 10% conversion to the *mer*-isomer is observed but the corresponding Mn(diimine)(CO)$_3$Cl containing MOF, {Mn(DMF)$_2$[(**1**)Mn(CO)$_3$Cl]}$_n$ **MnMn**, undergoes 25% conversion from the *fac*- to the *mer*-isomer. This level of isomerisation allows direct characterisation of the product by single crystal X-ray diffraction experiments[17] and demonstrates that through suitable design it is possible to investigate such photo-initiated structural transformations within MOFs.

Upon replacing the Mn(II) metal cation nodes of the MOF with the potentially redox-active Cu(II) it is possible to make [{Cu(DMF)(H$_2$O)[(**1**)Re(CO)$_3$Cl]}•DMF]$_\infty$ **ReCu** (Figure 1b),[19] which has a different overall topology to both **ReMn** and **MnMn**. Photo-irradiation of this complex results in an irreversible photoinduced charge transfer process. Following laser excitation, a ^{3}MLCT excited state is observed on a 3 ps timescale which decays rapidly concurrently with partial reformation of the parent bands and with formation as a new species with bands shifted to lower energy, relative to the parent bands, consistent with formation of an intraligand (IL) $^3\pi$-π^* excited state. These results are similar to those found when studying the **ReMn** MOF under the same conditions. However, when the TRIR experiments are undertaken for prolonged periods of time, marked differences are observed between **ReMn** and **ReCu**. Whereas the **ReMn** network is completely photostable, under the conditions used, the **ReCu** network shows small but important differences following cycles of photo-excitation. New infra-red bands began to appear, primarily at slightly higher energy than the parent ν(CO) bands, consistent with the gradual and irreversible formation of a low quantum yield photoproduct. The irreversible formation of a new photoproduct ultimately allows the use of low power laser light to selectively induce the irreversible photo-induced process enabling optical 'writing' on a single crystal.
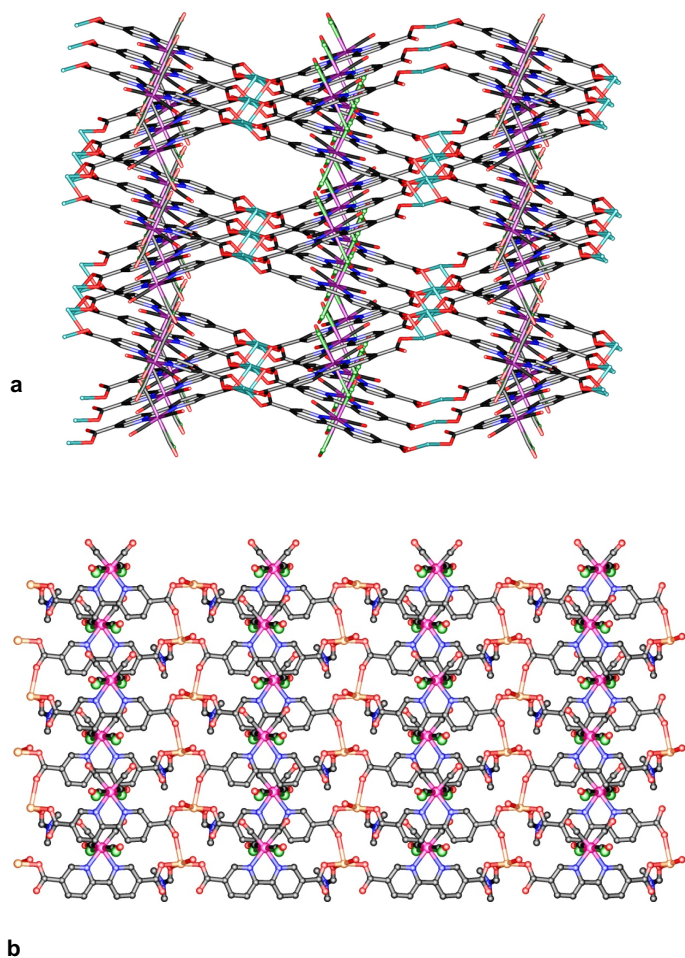
Figure 1. Views of the single crystal X-ray structure of a) **ReMn**, indicating the interlinking of [Mn(carboxylate)]$_\infty$ chains by (diimine)Re(CO)$_3$Cl moieties; b) **ReCu** viewed along the crystallographic *a*-axis illustrating the five-coordinate geometry of the Cu(II) cation. Mn, Light blue;, Re, purple; C, grey; O, red; N, blue; Cl, green; Cu, orange. In all figures hydrogen atoms and DMF molecules have been omitted for clarity. Figure 1a: Reproduced with permission from Ref. 17. Copyright Nature Publishing Group, 2010; Figure 1b: Reproduced with permission from Ref. 19. with permission from The Royal Society of Chemistry.

Results and Discussion

As described above, the use of MOF frameworks opens up the potential use of these materials as platforms to probe photochemical processes by IR time-resolved measurements.[20] Given we have characterized the *fac*- to *mer*-Mn(diimine)(CO)$_3$X isomerization in a Mn carboxylate MOF (**MnMn**)[17] we have investigated further the photochemistry of **MnMn** with fast time-resolved IR with a view to potentially using these materials as precursors for time-resolved

X-ray measurements which would allow the isomerization to be monitored in real time.
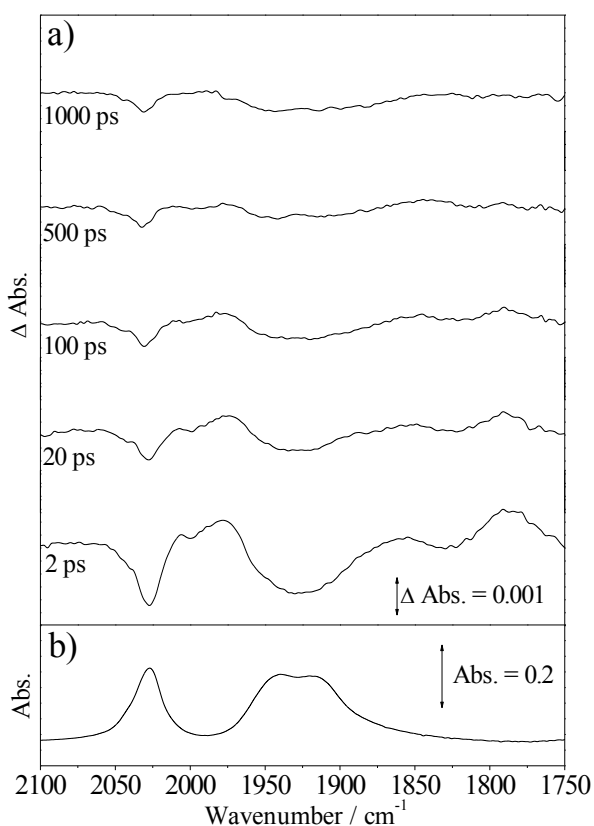

Figure 2. a) ps-TRIR difference spectra recorded following 400 nm irradiation of **MnMn** in a KBr disc, showing initial formation and subsequent decay of a CO loss intermediate. b) FTIR spectrum of **MnMn** in a KBr disc.

The ps-TRIR difference spectra obtained 1 ps following excitation of **MnMn** MOF in a KBr pellet is shown in Figure 2. It is clear that the parent ν(CO) bands at 2028, and 1941cm^{-1} are bleached and a new species is produced with two ν(CO) bands (1975 and 1970 cm^{-1}) shifted to lower wavenumber relative to the parent consistent with formation of the Mn(diimine)(CO)$_2$ moiety in the MOF framework. These bands are not stable and the TRIR spectrum taken after 500 ps clearly shows these bands have decayed. The behaviour of the dicarbonyl intermediates can be more easily visualised by examining the TRIR decay traces at the intermediate and parent absorption bands (Figure 3). It can be clearly seen that on the picosecond timescale the bands assigned to Mn(diimine)(CO)$_2$ moiety are not stable and decay (k_{obs} = 4.4 ($\pm$0.5) x10^{10} s^{-1}). This is initially surprising for several reasons; firstly our previous paper[17] examining the photoisomerisation by X-ray crystallography showed high conversion of *fac*- to *mer*-isomer of the Mn(diimine)(CO)$_3$X with the MOF which proceeds

through the dicarbonyl intermediate and it might be expected that a long-lived intermediate might be needed to effect efficient isomerisation. However, this is due to the difference in the two experiments as the X-ray measurements were obtained following cw irradiation which can build-up the desired photoproduct while the time-resolved experiments are performed following pulsed laser excitation and probes the events following the absorption of 1-photon. The second reason why the rapid decay of the $Mn(diimine)(CO)_2$ moiety was surprising is that similar dicarbonyl nominally 16-electron intermediates such as $CpMn(CO)_2(alkane)$ live for much longer timescales (>100 μs) in solution at room temperature.[21] Further insight into the short lifetime comes from examining the TRIR trace at the parent $\nu(CO)$ band. It can clearly be seen from Figure 2 that the parent is reformed (*ca.* 80%) at the same rate ($k_{obs} = 4.4$ (±0.6) $\times10^{10}$ s^{-1}) as the bands assigned to $Mn(diimine)(CO)_2$ decay. Furthermore, the bands due to $Mn(diimine)(CO)_2$ do not fully decay and there is a ca. 20% residual absorption. These results show that the majority of the photo-ejected CO does not escape from the vicinity of the metal centre and thus is *trapped* in the channel and there is rapid recombination of this trapped CO on the picosecond timescale. This may be due, in part, to packing of solvents in the channels and the rapid recombination of CO in the **MnMn** MOF means it is not ideal for study for generating long-lived unsaturated intermediates.
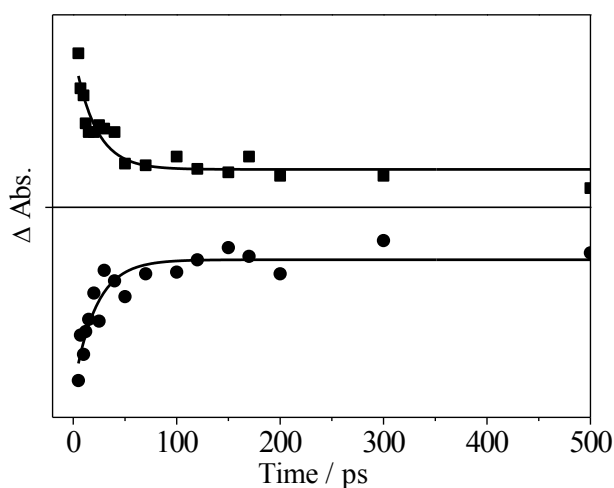

Figure 3. Picosecond kinetic traces taken from TRIR spectra recorded following 400 nm excitation of **MnMn** in a KBr disc, showing decay of the CO loss product at 1802 cm^{-1} (circles) and reformation of the parent species at 2016 cm^{-1} (squares). Solid lines indicate monoexponential fits.

Given the rapid CO recombination observed for the **MnMn** MOF we decided to explore the possible effect of modifying the structure and properties of the MOF through

changing the framework-propagating cation from a di-positive, potentially redox-active, transition metal cation [Mn(II)[17] or Cu(II)[19]] to a mono-positive, redox-inert, cation; in our case Li(I) cations. In addition to modifying the nature of the interaction between the carboxylate groups and the framework-propagating cation but in addition two mono-positive cations are required to balance the charge that is balanced by a single cation in the case of Mn(II) or Cu(II), potentially leading to structural variations of the framework. Thus, we were interested to probe the effect of modifying the constituents of the framework upon the photochemistry of the Mn or Re-dimine species supported by the MOF.

Synthesis and Characterisation of ReLi and MnLi.

The reaction of either Re($\mathbf{1}$H$_2$)(CO)$_3$Cl or Mn($\mathbf{1}$H$_2$)(CO)$_3$Br with either LiCl or LiBr, respectively, in a 1:1 mixture of DMF and acetonitrile at 80 °C in a pressure tube for 2 days produces yellow (**ReLi**) or orange (**MnLi**) crystals, of uniform morphology, of the target MOFs. Single crystal X-ray diffraction studies revealed the three-dimensional structures of the MOFs, **ReLi and MnLi** and confirm that the two frameworks are isostructural.

The networks consist of one-dimensional chains of carboxylate-bridged Li(I) cations aligned to the crystallographic *a*-axis that are cross-linked by individual units of Re($\mathbf{1}$)(CO)$_3$Cl (**ReLi**) or Mn($\mathbf{1}$)(CO)$_3$Br (**MnLi**). As anticipated, the Re(I), or Mn(I), centres retain a pseudo-octahedral geometry and the *fac*-CO arrangement (Figure 4) as seen in the starting materials Re($\mathbf{1}$H$_2$)(CO)$_3$Cl or Mn($\mathbf{1}$H$_2$)(CO)$_3$Br. The bond lengths and angles around the Re(I) or Mn(I) metal cations are consistent with literature values.[22,23] In both instances, the symmetry of the crystal structure results in the halide ligand and the axial CO ligand (perpendicular to the plane of the bipyridyl rings) being disordered with occupancies of 0.5 in both positions.

In both **ReLi** and **MnLi** the Li(I) cations are coordinated by three separate carboxylate donors and the oxygen atom of a DMF molecule in a highly distorted tetrahedral geometry. Each bridging carboxylate group adopts a μ^3 bridging mode, with one oxygen donor coordinating to only one Li(I) cation and another bridging two Li(I) cations (Figure 5a). As a result of this binding mode, the one-dimensional chains consist of fused and alternating 4- and 8-membered rings (Figure 5b), a motif similar to that observed by Clegg and Russo in the crystal structure of a Li salt of isophthalic acid (*m*-C$_6$H$_4$(COOH)(COOLi)).[24] Considering each Li centre as an individual 3-connected node and Re($\mathbf{1}$)(CO)$_3$Cl as a 6-

connected node, the Schläfli symbol for the net is $2[4^2.6]$ and $[4^4.6^2.8^8.10]$ for the Li and Re($\mathbf{1}$)(CO)$_3$Cl nodes respectively. Thus both **ReLi** and **MnLi** adopt an **alb** topology.[25]

Viewing both **ReLi** and **MnLi** along the *a*-axis (Figure 6a) reveals that its overall structure is almost identical to that of **ReMn**,[17] even though their topologies, along with the number of metal nodes and their coordination modes, are completely different. Each 4-membered [Li$_2$(μ^2-O)] ring of **ReLi**, or **MnLi** (Figure 6b), is effectively the topological equivalent of a Mn(II) centre in **ReMn**, coordinating 4 carboxylates and two DMF molecules. Both networks can be thought of as 1D chains of metal nodes [Li(I) or Mn(II)] linked by units of Re($\mathbf{1}$)(CO)$_3$Cl, or Mn($\mathbf{1}$)(CO)$_3$Br. As a result chains of $\{$[Re($\mathbf{1}$)(CO)$_3$Cl]Li$_2\}_n$, or $\{$[Mn($\mathbf{1}$)(CO)$_3$Br]Li$_2\}_n$, are formed which are aligned along the diagonals of the crystallographic *bc*-plane and, using the planes of the bipyridine rings as references, the angle between the two sets of chains is similar in all three networks (**ReLi**, ~40 °; **MnLi**, 40.8 °; **ReMn**, 39.5 °) (Figure 6c).

The majority of three-dimensional Li-based coordination polymers consist of two-dimensional sheets of carboxylate-bridged Li(I) cations, with the sheets connected by ligands containing two carboxylate groups. A useful comparison to **ReLi**/**MnLi** is the structure formed by the Li salt of biphenyl-4,4'-dicarboxylic acid (H$_2$biph), Li$_2$(biph) (ULMOF-2), a linker of the same length as $\mathbf{1}$, reported by Banerjee *et al.*[26] Within the two-dimensional sheets of Li-carboxylate moieties in ULMOF-2 contain one-dimensional chains of fused and alternating 4- and 8-membered rings similar to those observed in **ReLi**/**MnLi** (Figure 5c). In the case of ULMOF-2, however, the coordinated DMF molecules found in **ReLi**/**MnLi** are replaced by an O atom from a carboxylate group of a neighbouring 1D chain, resulting in a μ^4 binding mode for each carboxylate (μ^2 for each O atom). Extended throughout the whole structure, this results in the 1D chains being fused together by 6-membered rings to form the 2D sheets (Figure 5c). These are linked by close-packed biph units to form a non-porous three-dimensional coordination network.[26]

Comparing the structures of **ReLi**/**MnLi** and ULMOF-2, it is straightforward to understand why they form different networks. Although the two linkers are almost identical in length, Re($\mathbf{1}$)(CO)$_3$Cl has far more steric bulk than biph, which means the bipyridine moieties cannot close-pack in the same way as the biphenyl rings in ULMOF-2; therefore 2D sheets of Li(I) cations cannot be formed in **ReLi**/**MnLi** resulting in one-dimensional Li-carboxylate chains and the resulting 3D structure.
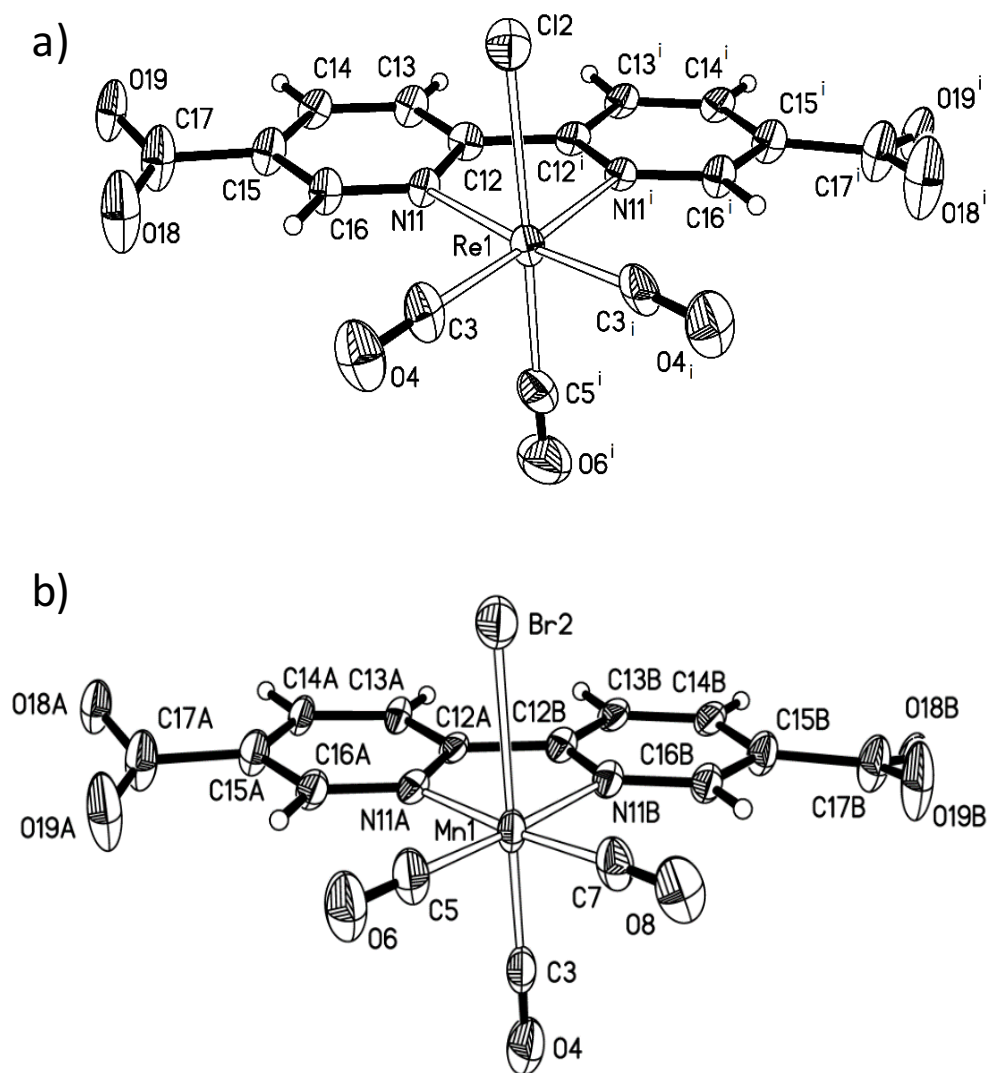
Figure 4: Coordination environments of a) Re(I) centre observed in **ReLi**, showing the numbering scheme used. Symmetry codes: i) +x, 1.5-y, -0.5-z. b) Mn(I) centre observed in **MnLi**, showing the numbering scheme used. Displacement ellipsoids drawn at 50% probability level.
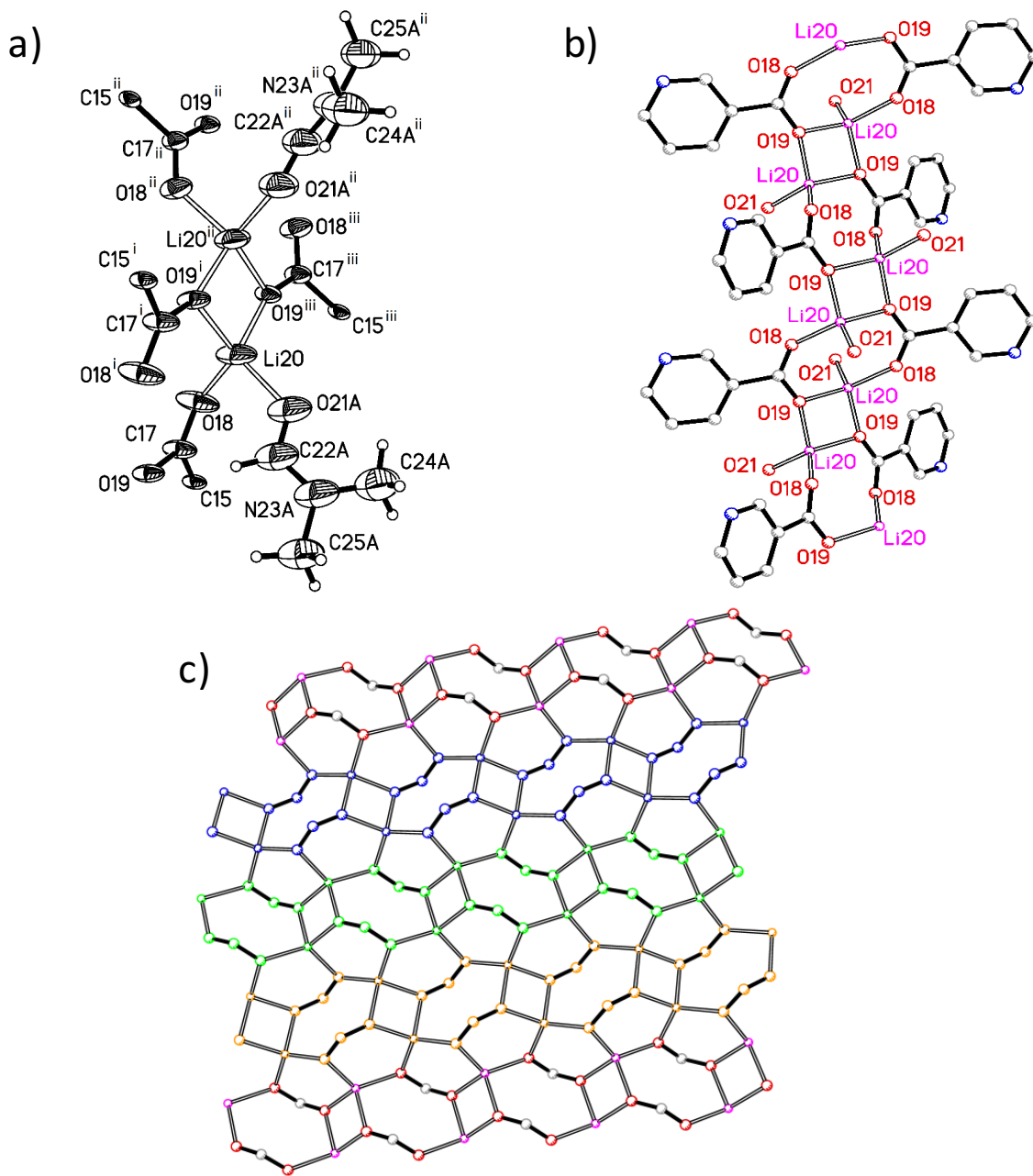
Figure 5: a) Environment of Li centres observed in **ReLi**, showing the coordinated carboxylate groups and DMF molecules, along with the numbering scheme used. **MnLi** adopts an isostructural arrangement. Displacement ellipsoids drawn at 50% probability level. Symmetry codes: i) 1-x, 1-y, -z; ii) 0.5-x, 1-y, +z; iii) -0.5+x, +y, -z. b) The 1D chains of carboxylate-bridged Li centres formed in **ReLi**. Hydrogen atoms and coordinated DMF molecules apart from their oxygen atoms are omitted for clarity. (Li = magenta, C = grey, N = blue, O = red). c) Two-dimensional sheet of carboxylate-bridged Li centres formed by ULMOF-2[26] with one-dimensional chains of 4- and 8-membered rings, as seen in **ReLi** and **MnLi**, highlighted in orange, green and blue.
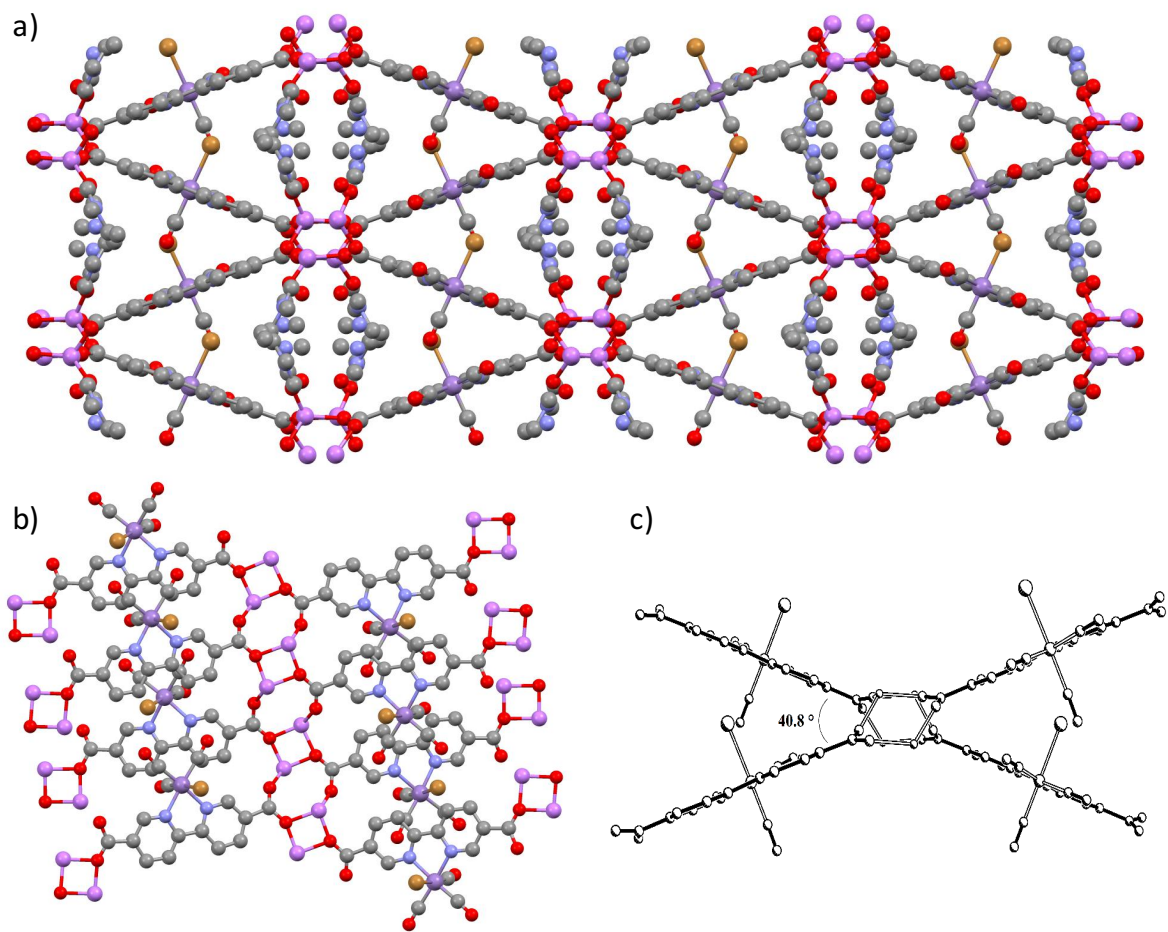
Figure 6: Views of the three-dimensional framework structure of **MnLi** along a) the crystallographic *a*-axis; b) the crystallographic *c*-axis. c) View highlighting the angle formed between $\{[Mn(\mathbf{1})(CO)_3Br]Li_2\}_n$ chains in **MnLi**. Hydrogen atoms are omitted for clarity and in b) and c) the DMF molecules are also omitted. (Br = brown, Li = magenta, C = grey, N = blue, O = red, Mn = purple).

TRIR and Luminescence Studies of ReLi and MnLi.

The photophysics of the metal-organic framework **ReLi** was initially studied using emission spectroscopy. Thus, a powder of **ReLi** was studied by luminescence spectroscopy. Upon excitation (406 nm) a broad, featureless emission is observed at 614 nm which is consistent with formation of a Re→diimine ^{3}MLCT excited state (Figure 7). The unsubstituted [Re(bipy)(CO)$_3$Cl] has an emission of 642 nm in 2-methyltetrahydrofuran (MeTHF) while the 4,4'-CO$_2$Me substituted analogue emits at a lower energy at 715 nm, which can be attributed to the electron-withdrawing nature of the CO$_2$Me substituents lowering the energy of the bipy π^* orbital.[27] The higher energy emission from the MOF could possibly because in this environment solvent stabilisation of the MLC. For example, the emission from [Re(CO)$_3$Cl(4,4,'-bipy(CO$_2$Et)$_2$)] in a MeTHF glass at 77K is at 598 nm.[27]

As the emission energy of **ReLi** is more similar to unsubstituted [Re(bipy)(CO)$_3$Cl], this could indicate that lithiation or the structural effects of the MOF appear to raise the energy of the unoccupied bipy orbital relative to that of the discrete linker complex particularly the emission lifetime (τ = 22 ($\pm$2) ns) is comparable to that of unsubstituted [Re(bipy)(CO)$_3$Cl] in solution.[27]
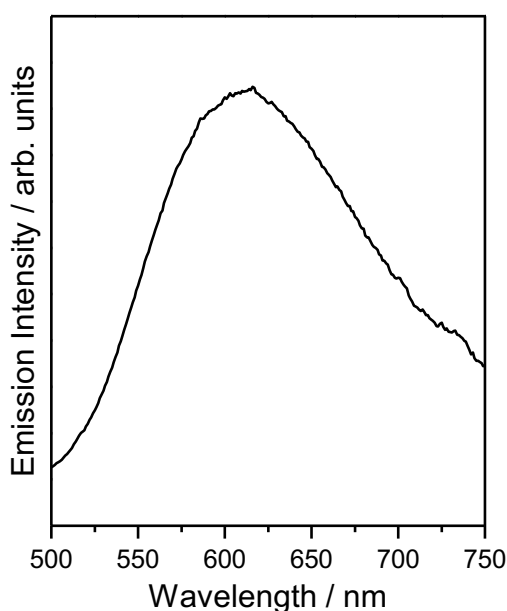

Figure 7: Emission spectrum of **ReLi** following excitation at 406 nm.

These results are in direct contrast to **ReMn** and **ReCu** where no observable luminescence was observed.[17,19] Although emission spectroscopy provides information on the nature of the emissive excited state, it does not probe the non-emissive, dark, state. We have also carried out DFT calculations on model linker complexes in order to estimate the electronic effects of the lithium or manganese subunits on the bipyridine π^* orbitals. The model compounds considered are [Re(bipy)(CO)$_3$Br] (**Rebpy**), [Re(**1**H$_2$)(CO)$_3$Br] (**ReCOOH**), and the bis-5,5'-(CO$_2$Li(DMF)$_2$) substituted analogues (**ReLi$_2$**). Figure 8 shows a plot of the energies of the highest occupied and unoccupied MOs, which are based on the metal and the bipy respectively. As expected, the HOMO-LUMO gap is decreased with respect to the unsubstituted complex upon substitution with CO$_2$H; this is reversed by the addition of the lithium-DMF moiety. Although the use of the HOMO-LUMO gap is a somewhat simplistic model for the excited state energy it indicates that the energies of emission (and therefore MLCT excited states) of these complexes are consistent with the electronic natures of the substituents. However, this simplistic model does not account for structural changes imposed by the MOF environment but the large increase calculated upon lithiation does suggest that this coordination is a dominating factor in switching on luminescence in these MOFs compared to the related **ReMn** MOF.
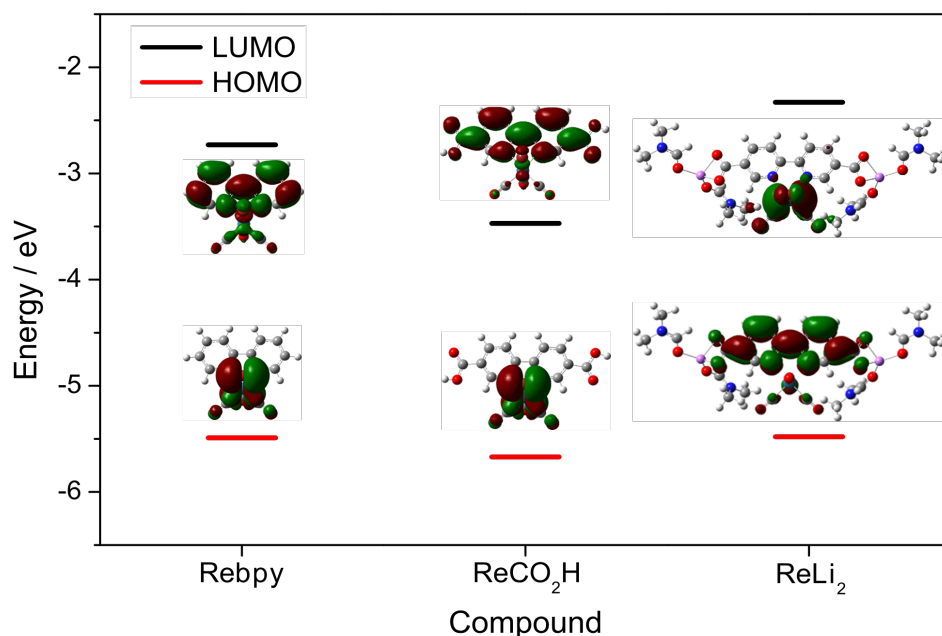

Figure 8: Energies of equivalent MOs of model linker compounds calculated at the B3LYP level of theory with the LANL2DZ basis set for Re and 6-31g(d) for other atoms.

For the non-emissive MOFs **ReMn** and **ReCu**, fast TRIR spectroscopy showed that MLCT followed by decay of the MLCT state to form IL (intraligand) π-π* excited states were observed for both materials. Thus, we have investigated the photophysics of **ReLi** using both the picosecond and nanosecond timescales by TRIR spectroscopy. Figure 9 shows a series of TRIR difference spectra recorded following 400 nm irradiation of **ReLi** in a KBr matrix. Upon irradiation, the ground state ν(CO) bands were bleached (1865, 1915 and 2005 cm^{-1}), and three new transient bands were observed. These bands appear at higher energy relative to the parent ν(CO) bands consistent with the formation an ^{3}MLCT excited state (1941, 1970 and 2043 cm^{-1}). These new bands narrow and shift to higher energy over the first 5 ps following irradiation consistent with vibrational relaxation of the excited state complex. The assigned ^{3}MLCT state is very stable and only partially decays to reform the parent on the picosecond timescale. The ns-TRIR difference spectra obtained 1 ns following excitation (355 nm) of **ReLi** in a KBr disc shows ^{3}MLCT excited state is still present (Figure 9). The ^{3}MLCT state decays (τ = 19 ($\pm$4) ns) to reform the parent, and growth of another excited state with three ν(CO) bands (1858 and 1997 cm^{-1}, a third band at approximately 1900 cm^{-1} is obscured by the parent bleaches). The decay of the IR bands assigned to the MLCT excited state occurs with the same lifetime obtained from emission spectroscopy and provides further support for the assignment of these bands to be due to a MLCT state. The new state which grows in as the MLCT excited state decays, appears at lower energy with respect to the parent and consistent with formation an IL π-π* excited state similar to the previously reported behaviour for **ReMn** and **ReCu** (see Table 1).[17,19] The decay of the MLCT to form the π-π* excited state is more clear in the TRIR decay trace, Figure 10(a). The IL state then decays to reform the ground state parent (τ = 335 ($\pm$25) ns). Only a small proportion of the ^{3}MLCT excited state decays to form the IL state, suggesting a higher energy of the IL state, at a significantly lower rate than the equivalent states of **ReMn** and **ReCu**. This suggests that there is a decreased driving force for the MLCT to IL interconversion for **ReLi**.

The excited state behaviour of **ReLi** appears to be closer to the behaviour of [Re(bipy)(CO)$_3$Cl] in solution than that of **ReMn**, showing a longer-lived and emissive ^{3}MLCT excited state, which decays on the nanosecond timescale. The timescales for both the interconversion between MLCT $\rightarrow$ π-π* excited states (τ_1) and the subsequent decay of the intraligand state (τ_2) differs for each of these materials with the orders **ReMn** (τ_1 = 20 ps; τ_2= 23 ($\pm$5) ns) > **ReCu** (τ_1 = 20 ps; τ_2= 19 ($\pm$3) ns)> **ReLi** (τ_1 = 20 ns; τ_2= >1 μs). The differences in the photophysics of **ReLi** to **ReMn** and **ReCu**, as well as the presence of the IL

π-π* state at an energy below the MLCT state, may be an indirect reflection of the coordination environments around the linker metal. The resulting strains exhibited on the bipy by the MOF structures may change the torsional angle between the pyridine rings, which is expected to significantly affect the conjugation and therefore the energies of the ligand-centred orbitals.
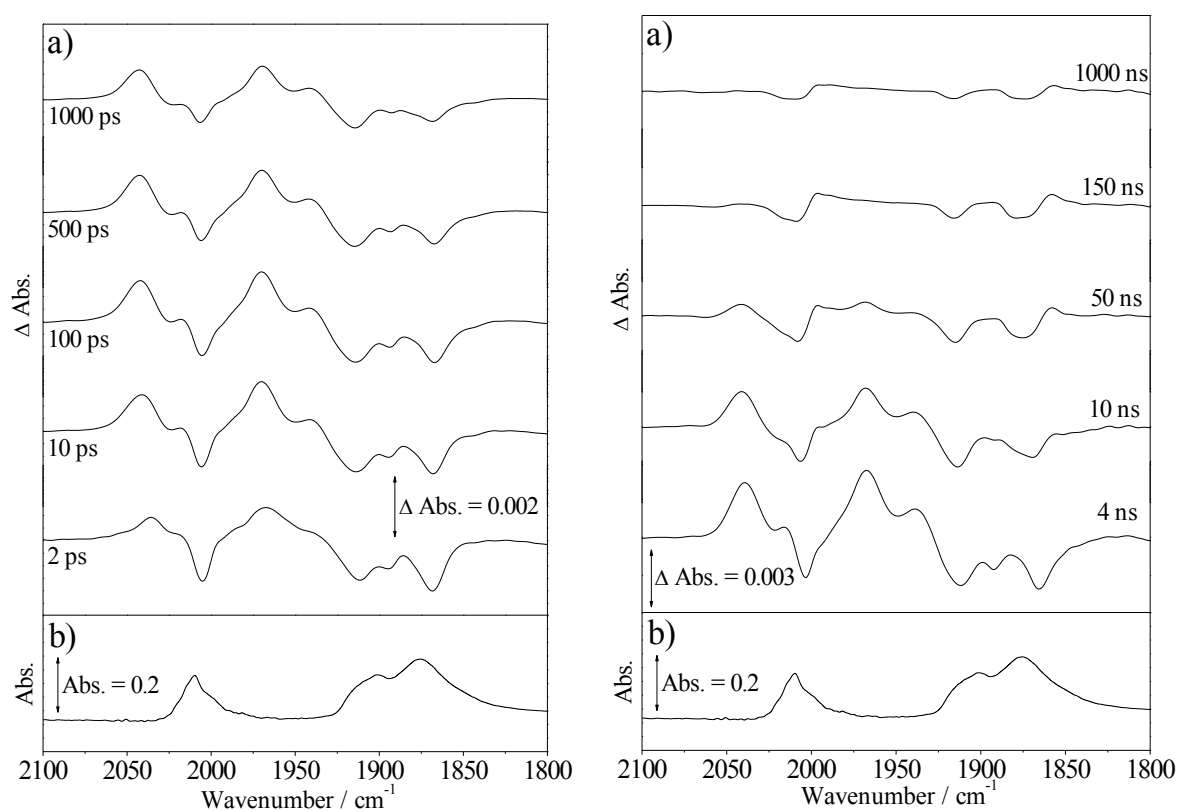

Figure 9: (a) ps-TRIR difference spectra obtained following 400 nm irradiation of **ReLi** in a KBr disc, showing formation of an MLCT excited state on the picosecond timescale. b) FTIR of the same KBr disc containing **ReLi**.
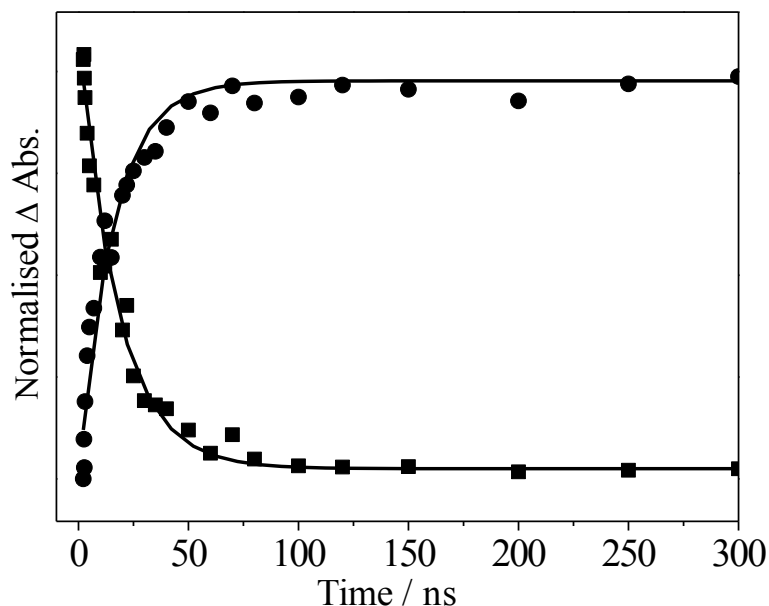
Figure 10: Nanosecond kinetic traces from TRIR difference spectra recorded at 1997 cm^{-1} (squares) and 2043 cm^{-1} (circles) following 355 nm irradiation of **ReLi** in KBr, showing decay of the ^{3}MLCT excited state, and growth of the π-π^* IL state.

It is clear that **ReLi** showed significantly different photophysics compared to **ReMn** and **ReCu** and here we examine the difference in photochemistry between **MnLi** and **MnMn** using TRIR spectroscopy. Upon irradiation of **MnLi**, the three ground state parent $\nu(CO)$ bands bleach (2022, 1936 and 1909 cm^{-1}) and two transient bands (1967 and 1802 cm^{-1}) form at lower energy relative to the parent bands. The number and position of $\nu(CO)$ bands for this intermediate suggests a dicarbonyl species. The dicarbonyl species quickly recombines with the dissociated CO, which is held in close proximity by the MOF structure analogous to the experiments performed on **MnMn**. The decay of the dicarbonyl (τ = 75 ($\pm$7) ps) is accompanied by growth of a transient band at 2016 cm^{-1} (Figure 10). The kinetics of this process are shown in Figure 12. The decay of the dicarbonyl species is also concurrent with reformation of the parent bands, leading to 80% parent recovery after 300 ps. This second transient species, however, is stable and does not decay to reform the ground state parent on this timescale.
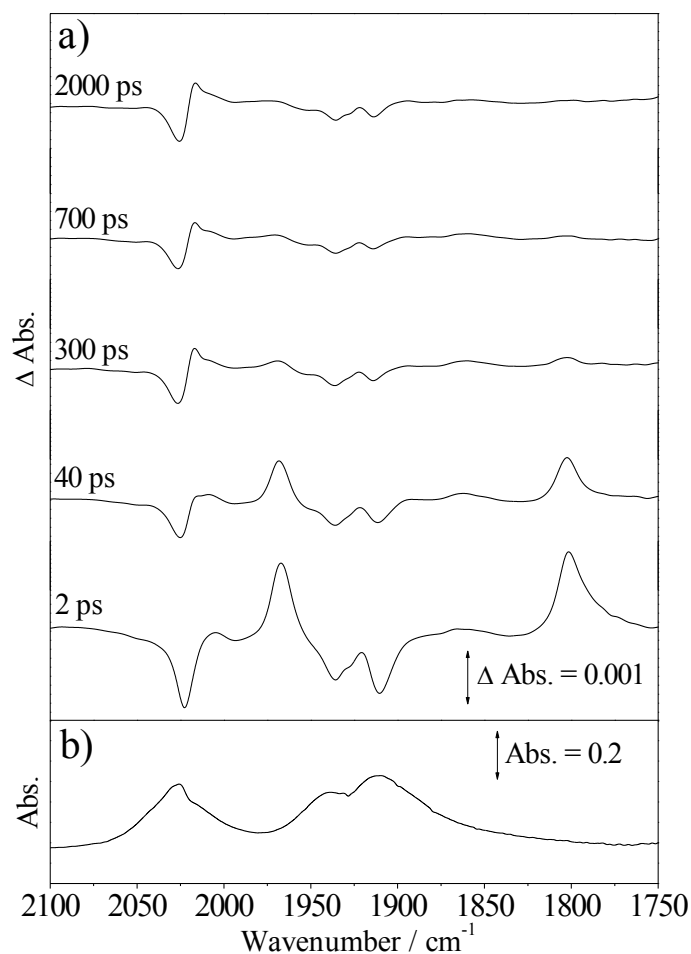
Figure 11: a) ps-TRIR difference spectra recorded following 355 nm irradiation of **MnLi** in a KBr disc, showing initial formation and subsequent decay of a CO loss intermediate. Decay of this CO loss species is accompanied by growth of an additional new transient species which is stable on the picosecond timescale. b) FTIR of **MnLi** in a KBr disc.

The recombination process observed for **MnLi** is still consistent with the majority of the photoejected CO not escaping the channel and rapidly reacting to reform a tricarbonyl species. However, the rate of recombination observed for **MnLi** (τ = 75 ($\pm$7) ps) is slightly slower than that observed for **MnMn** (τ = 23 ($\pm$5) ps) but much less than expected from a dicarbonyl and consistent with rapid recombination of CO trapped in the channel. This is consistent with the observation that there appears from the X-ray data that there is little difference between the two MOF structures in terms of the solvent occupancy of the MOF channels.
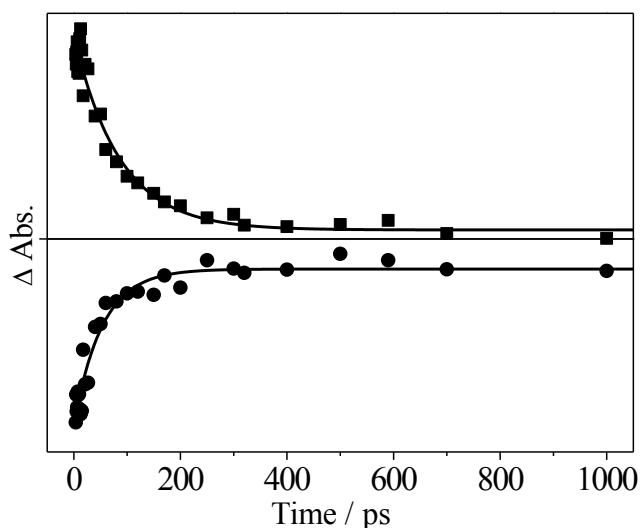
Figure 12: Picosecond kinetic traces taken from TRIR spectra recorded following 400 nm excitation of **MnLi** in a KBr disc, showing decay of the CO loss product at 1802 cm^{-1} (circles) and reformation of the parent at 2022 cm^{-1} (squares). Solid lines indicate monoexponential fits.

Conclusions

In this study we have shown that it is possible to synthesise new members of a family of MOFs, {M'[(**1**)M(CO)$_3$X]}$_n$, which support M(CO)$_3$X(diimine) moieties on the framework structure. We have investigated the effect of changing the framework-propagating metal cation from transition metals used in previous studies, Mn(II)[17,18] or Cu(II)[19], to an alkali metal, in this case Li(I). The overall framework structure of the MOF, for either **ReLi** or **MnLi**, remains highly similar to that observed for the Mn(II)-containing analogues **MnMn** or **ReMn**,[17,18] despite replacing a single di-cation, Mn(II), with two mono-cations. It is interesting to observe that despite the similarity of the framework structures the lithium-containing MOFs exhibit quite distinct photophysical and photochemical behaviour. The clearest distinction is that **ReLi** exhibits luminescence in direct contrast to **ReMn** and **ReCu** for which no luminescence was observed. DFT calculations reveal that the HOMO-LUMO gap in the Li-substituted [(**1**)M(CO)$_3$X] moiety is increased with respect to the parent carboxylic acid-functionalised species and is more similar to unsubstituted [Re(bipy)(CO)$_3$Cl]. Indeed, the emission energy of **ReLi** is similar to that exhibited by unsubstituted [Re(bipy)(CO)$_3$Cl].

Time-resolved IR measurements were used to probe the nature of the exited states in **ReLi** and **MnLi** in comparison to **ReMn** and **MnMn**. The excited state behaviour of **ReLi** is closer in behaviour to that of unsubstituted [Re(bipy)(CO)$_3$Cl] in solution than that of **ReMn**. Upon excitation **MnLi** forms a dicarbonyl species which rapidly recombines with the dissociated CO in an analogous fashion to **MnMn**. As with **MnMn**, the behaviour of **MnLi** is consistent with the majority of the photoejected CO not escaping the MOF channels. The similar behaviour observed between **MnMn** and **MnLi** is consistent with the similarity between the two framework structures. In summary, we have demonstrated that simple variation in the components of the MOF it is possible to modify the photochemical behaviour of the MOF-supported components without changing the overall framework structure. Such simple modifications reveal great promise for tuning the behaviour of photochemically active MOFs.

Experimental Section

Materials and General Methods

Anhydrous THF and toluene were dried were dried over silica columns and degassed with N$_2$ for 30 minutes. All other chemicals and solvents were purchased from commercial sources and were used as received without any further purification. ^{1}H NMR and ^{13}C NMR spectra were obtained using a Bruker DPX 300 spectrometer or a Bruker DPX400 spectrometer; residual signals of solvent were used for reference. Electrospray ionisation mass spectra were collected using a Bruker Daltonics microTOF mass spectrometer. 2,2'-dipyridyl-5,5'-dicarboxylic acid,[28,17] *fac*-(2,2'-bipyridine-5,5'-dicarboxylic acid)tricarbonylchlororhenium(I)[17] and *fac*-(2,2'-bipyridine-5,5'-dicarboxylic acid)bromotricarbonylmanganese(I)[17] were prepared according to literature methods.

ReLi. A mixture of Re(**1**H$_2$)(CO)$_3$Cl (11 mg, 2 x 10^{-5} mmol) and lithium chloride (5 mg, 1 x 10^{-4} mmol) in DMF (1.3 mL) and acetonitrile (0.7 mL) was heated at 80 °C in a pressure tube for 3 days. Yellow crystals of **ReLi**, of a single morphology, were separated by filtration, washed with DMF and dried *in vacuo*. The product was fully characterised by single crystal X-ray diffraction. (Yield 35%). FTIR (KBr): ν(CO) 2005 (s), 1915 (s), 1865 (s), cm^{-1}; 2931 (w), 1664 (s), 1616 (s), 1406 (s), 1383 (m), 1295 (m), 1253 (m), 1134 (m), 1103 (w), 857 (m), 778 (s), 713 (m), 674 (m), 533 (m) cm^{-1}.

Crystal data for **ReLi**: $C_{21}H_{20}Li_2N_4O_9ClRe$. Orthorhombic, space group *Pnna*, a = 9.7376(4), b = 26.5692(11), c = 9.9267(4) Å, V = 2568.24(18) Å^3, Z = 4, D_{calc} = 1.831 g cm^{-3}, μ = 10.712 mm^{-1}, $F(000)$ = 1376. A total of 10173 reflections were collected, of which 2267 were unique, with R_{int} = 0. 0598. Final R_1 (wR_2) = 0. 086 (0.226) with GOF = 1.15.

MnLi. A mixture of Mn(**1**H_2)(CO)$_3$Br (9 mg, 2 x 10^{-5} mmol) and lithium bromide (10 mg, 1 x 10^{-4} mmol) in DMF (1.3 mL) and acetonitrile (0.7 mL) was heated at 80 °C in a pressure tube for 2 days. Orange crystals of **MnLi**, of a single morphology, were separated by filtration, washed with DMF and dried *in vacuo*. The product was fully characterised by single crystal X-ray diffraction. (Yield 35%). FTIR (KBr): ν(CO) 2022 (s), 1936 (s), 1909 (s) cm^{-1}; 2929 (w), 1690 (s), 1634 (s), 1609 (s), 1590 (s), 1365 (m), 1107 (m), 843 (m), 777 (s), 696 (m), 668 (m), 634 (m), 529 (m) cm^{-1}.

Crystal data for **MnLi**: $C_{21}H_{20}BrLi_2MnN_4O_9$. Orthorhombic, space group *Pnn2*, a = 9.6720(4), b = 26.6242(10), c = 9.9082(4) Å, V = 2551.46(18) Å^3, Z = 4, D_{calc} = 1.617 g cm^{-3}, μ = 6.544 mm^{-1}, $F(000)$ = 1248. A total of 4736 reflections were collected, of which 4029 were unique. Final R_1 (wR_2) = 0.010 (0.261) with GOF = 1.18.

Single-crystal X-ray diffraction

Single-crystal X-ray diffraction experiments were performed on an Oxford Diffraction SuperNova CCD area detector diffractometer operating at 90 K using mirror-monochromated Cu *K*α radiation (λ = 1.5418 Å). Gaussian grid face-indexed absorption correction with a beam profile correction (Crysalis Pro) was applied.[29] The structures were solved by direct methods using SHELXS[30] and refined by full-matrix least squares on F^2 using SHELXL.[30] Both structures contained significant disorder and in the case of **MnLi**, the crystal was found to be twinned.

TRIR Measurements

Picosecond and nanosecond TRIR measurements were performed at the ULTRA ultrafast infrared absorption facility at the Rutherford Appleton Laboratory, Harwell Oxford. The ULTRA system has been described in detail elsewhere.[32] A pulse of 50 fs duration and 0.8 mJ output is produced by a Ti:sapphire dual output amplifier (Thales Laser) with a repetition rate of 10 kHz, at 800 nm. This 800 nm beam is then split into two. The first section is used to generate a 400 nm UV pump pulse by second harmonic generation. The second is passed

through optical parametric amplifiers (TOPAS, Light Conversion) to produce the tuneable mid-IR probe beam. The IR probe beam is split into two to form probe and reference beams. After passing through the sample, the IR probe is dispersed onto two linear 128-element MCT array detectors (Infrared Associates). The 400 nm pump beam is focussed to a spot size of *ca.* 100 μm, and overlapped at the sample position with the mid-IR probe beam, which is focussed to *ca.* 80 μm. A small portion of the IR probe beam is dispersed onto a 64-element MCT array detector (Infrared Associates), acting as a reference. For nanosecond TRIR measurements, a separate nanosecond laser capable of providing 355 nm and 266 nm excitation pulses was utilised, which was delayed electronically.

Pump-on pump-off infrared absorption difference spectra were recorded at high speed (10 kHz). The two spectral windows were calibrated separately using the characteristic absorption lines of cis-stilbene. The overlapping spectral windows were interleaved using overlapping parent bleach signals recorded at the same delay time. The sample was rastered in the *x* and *y* directions during data acquisition.

Solid Sample Preparation for TRIR

Solid samples were made up as KBr discs. KBr (*ca.* 130 mg) was ground into a fine powder and mixed with sample material (*ca.* 5 mg). The mixture was then ground gently until homogeneous in colour. The mixture was placed into a 13 mm die and pressed in a hydraulic pellet press at 10 tons pressure for 20 minutes to form a disc of approximately 1 mm thickness. It was determined that KBr discs of 1 mm thickness represented an optimum balance between IR transmittance and the structural integrity of the disc. Sample discs were placed in a specially constructed windowless cell.

Density Functional Theory

All calculations were carried out using Gaussian09. Ground state optimisations were carried out using the B3LYP functional with the LANL2DZ basis set for rhenium and 6-31g(d) for all other atoms. Frequency calculations were performed to ensure that local minima were obtained.

Data Accessibility

The Supplementary Material contains additional figures of X-ray structures. CIF data have been deposited with the Cambridge Crystallographic Data Centre, CCDC reference numbers CCDC-1492830 (**MnLi**) and CCDC-1492831 (**ReLi**).

Competing interests

The authors declare that they have no financial or non-financial competing interests.

Authors' contributions

TJR prepared all materials. TJR and WL collected X-ray diffraction data and refined crystal structures. TSM., JAC, RH, IPC, GMG and MT collected and analysed time-resolved spectroscopic data. NRC and MWG conceived of the study, designed the study, coordinated the study. All authors drafted the manuscript and gave final approval for publication.

References

1. H. Furukawa, K. E. Cordova, M. O'Keeffe and O. M. Yaghi, *Science*, 2013, **341**, 1230444.
2. K. Sumida, D. L. Rogow, J. A. Mason, T. M. McDonald, E. D. Bloch, Z. R. Herm, T.-H. Bae and J. R. Long, *Chem. Rev.*, 2012, **112**, 724–781.
3. M. P. Suh, H. J. Park, T. K. Prasad and D.-W. Lim, *Chem. Rev.*, 2012, **112**, 782–835.
4. F.-K. Shieh, S.-C. Wang, C.-I. Yen, C.-C. Wu, S. Dutta, L.-Y. Chou, J. V. Morabito, P. Hu, M.-H. Hsu, K. C.-W. Wu and C.-K. Tsung, *J. Am. Chem. Soc.*, 2015, **137**, 4276–4279.
5. F. Lyu, Y. Zhang, R. N. Zare, J. Ge and Z. Liu, *Nano Lett.*, 2014, **14**, 5761–5765.

6. K. Liang, R. Ricco, C. M. Doherty, M. J. Styles, S. Bell, N. Kirby, S. Mudie, D. Haylock, A. J. Hill, C. J. Doonan and P. Falcaro, *Nat. Commun.*, 2015, **6**, 7240.

7. L. Sun, M.G. Campbell, and M. Dinca, *Angew. Chem. Int. Ed.* 2016, **55** ,3566 –3579

8. C. F. Leong, B. Chan, T. B. Faust and D. M. D'Alessandro, *Chem. Sci.*, 2014, **5**, 4724-4728.

9. Y. Inokuma, S. Yoshioka, J. Ariyoshi, T. Arai, Y. Hitora, K. Takada, S. Matsunaga, K. Rissanen, M. Fujita, *Nature*, 2013, 495, 461-466.

10. W.M. Bloch, N.R. Champness and C.J. Doonan, *Angew. Chem. Int. Ed.*, 2015, **54**, 12860-12867.

11. C. L. Jones , A. J. Tansell and T. L. Easun, *J. Mater. Chem. A*, 2016, **4**, 6714-6723.

12. R.N. Amador, M. Carboni, D. Meyer, *Mater. Lett.*, 2016, **166**, 327–338.

13. H. Reinsch, F.M. Hinterholzinger, P. Jäker, F. Hesse, B. Reimer, T. Bein, M. Položij, D. Nachtigallová, P. Nachtigall, and N. Stock, *J. Phys. Chem. C*, 2015, 119, 26401–26408; L.L. Gong, X.F. Feng, F. Luo, X.F. Yi and A.M. Zheng, *Green Chem.,* 2016, **18**, 2047-2055.

14. C. Wang, Z. Xie, K.E. deKrafft and W. Lin, *J. Am. Chem. Soc.*, 2011, **133**, 13445–13454.

15. R. Huang, Y. Peng, C. Wang, Z. Shi and W. Lin, *Eur. J. Inorg. Chem.* DOI: 10.1002/ejic.201600064.

16. H. Fei, M.D. Sampson, Y. Lee, C.P. Kubiak, and S.M. Cohen, *Inorg. Chem.*, 2015, **54**, 6821–6828.

17. A.J. Blake, N.R. Champness, T.L. Easun, D.R. Allan, H. Nowell, M.W. George, J. Jia and X.-Z. Sun, *Nature Chem.*, 2010, **2**, 688 - 694.

18. T.L. Easun, J. Jia, J.A. Calladine, D.L. Blackmore, C.S. Stapleton, K.Q. Vuong, A.J. Blake, N.R. Champness and M.W. George, *Inorg. Chem.*, 2014, **53**, 2606−2612.

19. T.L. Easun, J. Jia, T.J. Reade, X-Z. Sun, E.S. Davies, A.J. Blake, M.W. George and N.R. Champness, *Chem. Sci.*, 2014, **5**, 539-544.

20. J. A. Calladine, R. Horvath, A. J. Davies, A. Wriglesworth, X.-Z. Sun, M. W. George, *Appl. Spectr.* 2015 **69**, 519-524.

21. J.A. Calladine, S.B. Duckett, M.W. George, S.L. Matthews, R.N. Perutz, O. Torres, Q.V. Khuong, *J. Am. Chem. Soc.*, 2011, **133**, 2303-2310.

22. L.A. Garcia-Escudero, D. Miguel and J.A. Turiel, *J. Organomet. Chem.*, 2006, **691**, 3434-3444.

23. C. M. Alvarez, R. Garcia-Rodriguez and D. Miguel, *J. Organomet. Chem.*, 2007, **692**, 5717–5726.

24. W. Clegg and L. Russo, *Cryst. Growth Des.*, 2009, **9**, 1158-1163.

25. M. O'Keeffe, M.A. Peskov, S.J. Ramsden and O.M. Yaghi, *Acc. Chem. Res*. 2008, **303**, 1782-1789.

26. D. Banerjee, L.A. Borkowski, S.J. Kim, J.B. Parise, *Cryst. Growth Des.*, 2009, **9**, 4922-4926.

27. L.A. Worl, R. Duesing, P. Chen. L. Della Ciana and T.J. Meyer, *J. Chem. Soc., Dalton Trans.*, 1991, 849-858; P. Chen and T.J. Meyer, *Inorg. Chem.*, 1996, **35**, 5520-5524; P. Chen and T.J. Meyer, *Chem. Rev.*, 1998, **98**, 1439-1478.

28. C. Janiak, S. Deblon, H.-P. Wu, M.J. Kolm, P. Klüfers, H. Piotrowski and P. Mayer, *Eur. J. Inorg. Chem.*, **1999**, *9*, 1507-1522; X. Lin, I. Telepani, A.J. Blake, A. Dailly, C.M. Brown, J.M. Simmons, M. Zoppi, G.S. Walker, K.M. Thomas, T.J. Mays, P. Hubberstey, N.R. Champness and M. Schröder, *J. Am. Chem. Soc.*, **2009**, *131*, 2159-2171.

29. CrysalisPro, Oxford Diffraction Ltd.

30. G.M. Sheldrick, *Acta Cryst.,* 2008, **A64**, 112-122.

31. L. Spek, *Acta Cryst.*, 2009, **D65**, 148-155.

32. A. Vlcek, Jr., I. R. Farrell, D. J. Liard, P. Matousek, M. Towrie, A. W. Parker, D. C. Grills and M. W. George, *J. Chem. Soc. Dalton Trans*., 2002, **5**, 701-712.